ELSEVIER

Journal of Hazardous Materials 37 (1994) 327–352

JOURNAL OF HAZARDOUS MATERIALS

Modelling the effects of obstacles on the dispersion of denser-than-air gases

S. Andronopoulos[a,*], J.G. Bartzis[b], J. Würtz[a], D. Asimakopoulos[c]

[a] *Commission of the European Communities, Joint Research Centre, Safety Technology Institute, Process Engineering Division, I-21020, Ispra (Va), Italy*

[b] *National Centre for Scientific Research "Demokritos", Institute of Nuclear Technology and Radiation Protection, Gr-15310 Aghia Paraskevi, Attiki, Greece*

[c] *Department of Physics, Laboratory of Meteorology, University of Athens, 33 Ippokratous Str., Gr-10680 Athens, Greece*

(Received 16 March 1993; accepted in revised form 5 November 1993)

Abstract

The three-dimensional, finite volume code ADREA-HF is used to perform a computational simulation of the Thorney Island Dense Gas Trial No. 21. In order to avoid excessively fine discretisation to model the thin circular fence and still take into account the real shape and dimensions of the fence, a special technique is adopted: the computational cells which are in contact with the fence are characterised as "blocked" or "partially blocked". In the blocked cells, the flow is completely obstructed, while in the partially blocked cells, a flow resistance coefficient is evaluated. The above technique, in conjunction with a one-equation turbulence closure model gives rather satisfactory results in comparison with the experimental data in the form of concentration–time histories. The model has a tendency to underestimate the maximum gas concentration and the dose (integral of the concentration with time). The differences between model predictions and experimental data can be reduced by taking into account concentration fluctuations and possible improvements of the turbulence modelling.

1. Introduction

The code ADREA-HF [1, 2] was developed to compute the dispersion of denser-than-air vapour clouds with the aim of application to terrain of any complexity. It has already been applied in cases of dispersion over flat terrain [3–5] and this paper presents the first validation for the prediction of dispersion in the presence of obstacles. The code assumes a mixture of two fluids: the dense gas and the ambient air.

* Corresponding author. Present address: National Centre for Scientific Research "Demokritos", Institute of Nuclear Technology and Radiation Protection, Gr-15310 Aghia Paraskevi, Attiki, Greece.

SSDI 0304-3894 (93) E0108-E

It solves the conservation equations for the mixture total mass, momentum, energy and the mass fraction of the dense gas. A heat conduction equation for the layer adjacent to a solid boundary surface is also included. These equations are discretised, in the domain of interest, using a finite volume methodology, while several turbulence closure schemes are available in the code. For the computations presented in this paper, a one-equation turbulence model is utilised, since it was found adequate to describe the effects of an obstacle on the dispersion of a dense cloud.

The Thorney Island Heavy Gas Dispersion Trials (HGDT) were organised by the Health and Safety Executive (HSE, UK) in the framework of a research programme on the atmospheric dispersion of denser-than-air gases. Detailed information about the trials programme is given by McQuaid and Roebuck [6]. The primary objective of the trials was the acquisition of reliable data at large scale, in order to test the validity of mathematical and wind tunnel models for dense gas dispersion. The experiments of Phase II (10 trials) refer to the dispersion of fixed volume, isothermal clouds, in the presence of several different kinds of obstructions (impermeable fence, permeable screens and a rectangular building) under a variety of atmospheric conditions.

For the validation of the code ADREA-HF in the prediction of dispersion over obstacles, experiment no. 21 of the Phase II Thorney Island trials has been chosen for simulation. In this trial a semi-circular impermeable fence was placed around the gas source. The latter was a cylindrical container, the lateral sides of which were made of flexible plastic material. The container, filled with a mixture of Freon-12 and nitrogen, was placed at the centre of the semi-circular fence and at time 0.0 it collapsed rapidly to the ground, leaving a gas cylinder standing instantly still. In this respect, an instantaneous release was simulated. Trial 21 was chosen for simulation because, according to McQuaid and Roebuck [6], the release was fully successful and the interaction of the gas cloud with the fence was strong due to the relatively low wind speed.

During the experiment, gas sensors were placed on vertical masts to measure the dense gas concentration at several distances from the source and at several heights from the ground (0.4, 2.4, 4.4, 6.4 m). Other meteorological instruments, such as thermometers, cup- and sonic-anemometers, solarimeters, relative humidity sensors, wind vanes, smoke detectors and ultra-sonic gas sensors, were also placed on the masts, in order to measure the atmospheric conditions as well as turbulence characteristics during the dispersion of the cloud. Detailed information about the instrumentation of the trial can be found in the final report of the Trials Project [6].

2. Description of the mathematical formulation

2.1. The transport equations and the turbulence closure scheme

For the case of the Thorney Island Trial 21, the conservation equations of the total mass, momentum and mass of dense gas were solved by ADREA-HF, in the form presented in the appendix (Eqs. (A.1)–(A.3)), in a Cartesian coordinate system.

In the conservation equations the eddy viscosity–diffusivity approach is adopted to evaluate the turbulent fluxes, according to [1, 2] (see Eqs. (A.5)). For the computations described in this paper, the one-equation turbulence model described in detail in [2] (presented also in brief in Section 7.2) was used, with certain modifications which allow for:

(1) the application of the above turbulence model in the atmospheric surface layer (below 35 m), where the dispersion problem under consideration takes place,
(2) the modelling of the effect of thin, non-rectangular obstacles (such as the fence in Thorney Island Trial 21), without resorting to fine discretisation and
(3) the flow stability conditions which occur during dense gas dispersion and which are much stronger than those usually observed in the atmosphere [7].

The above modifications will be described in the following sections.

2.2. The turbulent momentum diffusion coefficients

In addition to the three components of the eddy viscosity K_{mi} $(i = x, y, z)$ along the three coordinate directions, as defined in [1] (see also Eq. (A.6)), an eddy viscosity K_{mn} along the direction $\hat{n}$ (where $\hat{n}$ is the unit vector normal to a surface of arbitrary orientation) is calculated as follows:

$$K_{mn} = C_\mu k^{1/2} l_n \tag{1}$$

where k is the turbulent kinetic energy, l_n is an effective length scale and C_μ (= 0.1887) is an empirical constant.

The turbulent kinetic energy k is computed by solving the transport equation, as given in [1] (see also Eqs. (A.7)–(A.11)).

Following the arguments presented in [2], the effective length scale l_n, to be used in Eq. (1), is calculated from

$$\frac{1}{l_n} = \left[\left(\frac{1}{l_{gn}} + \frac{1}{l_{sn}}\right)^r + \left(\frac{1}{l_0}\right)^r\right]^{1/r}, \quad r = 5 \tag{2a}$$

where l_{gn} is the wall length scale, equal to the shortest distance of the particular point from a solid boundary in the $\hat{n}$-direction, l_{sn} is a stability length scale in the $\hat{n}$-direction and l_0 is an "outer" length scale (see also Eq. (A.13)). These length scales are given by the relations:

$$l_{sn} = C_N \frac{k^{1/2}}{N_n} \tag{2b}$$

$$l_0 = C_\Gamma \frac{k}{\Gamma} \tag{2c}$$

$$\Gamma = \frac{1}{\rho}\left(\sum_i \left(\frac{\partial P}{\partial x_i}\right)_\infty^2\right)^{1/2} \tag{2d}$$

$$C_N = 0.51, \qquad C_\Gamma = 0.49$$

where N_n is the Brunt–Väisälä frequency in the $\hat{n}$-direction and $(\partial P/\partial x_i)_\infty$ is the asymptotic pressure gradient. The above model is based on the assumption that turbulence length scales mainly depend on the presence of solid boundary surfaces, local stability conditions and the global pressure acceleration field (Γ). It should be noted that the outer length scale has little influence, as long as the cloud remains close to the ground.

Following the reasoning presented in [1] (see also Eq. (A.14)), the Brunt–Väisälä frequency N_n in Eq. (2b) is defined as

$$N_n = \left[g_n \left(\frac{1}{\rho} \frac{\partial \rho}{\partial x_n} - \frac{c_v}{c_p} \frac{\rho}{P} g_n \right) \right]^{1/2} \tag{3}$$

As seen from Eqs. (2a)–(2c), the effective length scale in the horizontal direction is not affected by buoyancy since $g_n = 0$ in this direction. Thus, the horizontal length scale is mainly a function of the horizontal distance from the particular point to the nearest solid boundary surface. If this distance is very large, then so is the horizontal length scale. Thus, for points located far from solid boundaries in the horizontal direction, the horizontal diffusivities tend to assume large values and the model predicts a too large dilution rate of the dense gas cloud, leading to underprediction of the gas concentration. This deficiency was due to the fact that the original turbulence model was designed for use in the atmospheric Ekman layer and not in the surface layer where dispersion of dense gas occurs. It was faced by considering that the turbulent diffusivities in any direction for a particular point do not exceed a factor f times the smallest turbulent diffusivity for that point. This modification was adopted following Lantz et al. [8] who suggest that the ratio of the horizontal to the vertical turbulent diffusivities is a function of the stability of the ambient atmospheric flow expressed by the different Pasquill categories. Thus, for the present case, the following expressions are used:

$$K_{m,\min} \equiv \min(K_{mi(i=x,y,z)}, K_{mn}) \tag{4a}$$

$$K_{mi,\max} = f K_{m,\min} \tag{4b}$$

Preliminary calculations have shown that the results of the simulation are sensitive to the choice of the value of f. Lantz et al. [8] propose a value of 6 for the ratio of the horizontal to the vertical turbulent diffusivities for neutral atmospheric conditions, which was the case for Trial 21. In this respect $f = 6.0$ is adopted for Eq. (4) for this specific case.

2.3. *The turbulent Prandtl number*

The turbulent Prandtl number σ_h depends mainly on the flow stability and is used to calculate the turbulent mass diffusivity from the turbulent momentum diffusivity ($K_{\omega i} = K_{mi}/\sigma_h$). For unstable conditions, the relation for σ_h defined in [1] is adopted here (see Eq. (A.15)). For the stable case ($Ri \geqslant 0$), a fixed value of 0.72 is proposed in [1] for σ_h. The experimental data, on which this constant σ_h value is based, do not

extend over the strong stability conditions encountered during the dispersion of dense gases. It is worth noting that the calculations performed with $\sigma_h = 0.72$ for $Ri \geqslant 0$ resulted in high turbulent mass diffusivities and small dense gas concentrations. Furthermore, laboratory experiments conducted by Ellison and Turner [9] as well as atmospheric measurements under extreme stability conditions conducted by Kondo et al. [10], demonstrated that the turbulent Prandtl number increases with increasing stability. These experiments were performed with Richardson numbers from 0.0 to about 10.0, i.e. a range representative of the conditions during dense gas dispersion (Schreurs and Mewis [7]).

In the light of the above, the following relation, proposed by Ellison and Turner [9] to model the behaviour of the turbulent Prandtl number in stably stratified flows, is adopted here:

$$\sigma_h = Pr \frac{(1 - Ri_f)^2}{1 - Ri_f/Ri_{fc}} \quad \text{for } Ri \geqslant 0 \tag{5}$$

Here Pr is the classical Prandtl number, $Pr = \mu c_p/\lambda = 0.71$, and Ri_{fc} is the critical flux Richardson number, for which a value of 0.15 is assumed [9]. The physical meaning of the σ_h increase with increasing stability predicted by Eq. (5) is that in extremely stable stratifications the turbulent mass diffusivity tends to zero while the turbulent momentum diffusivity does not, since momentum can also be transferred by other means, as for example internal waves.

The validity of Eq. (5) is widely accepted and this equation has also been used by other modellers for dense gas dispersion [7, 11].

2.4. The numerical approach

Details on the numerical treatment of the transport equations solved by ADREA-HF are given in [1]. Here only the outline of the numerical procedure will be presented.

For the discretisation of the differential conservation equations, ADREA-HF uses a "control volume" formulation. The computational domain is divided into a number of non-overlapping finite control volumes (rectangular cells), over which the differential equations are integrated. For the control volumes of the velocity components, the "staggered grid" methodology is utilised.

For the time derivative, a first order, backward difference scheme is applied (fully implicit in time). In the convection terms the "upwind differencing" scheme is adopted, while in the diffusion terms "central differencing" is applied.

A discretised Poisson pressure equation is formed from the integrated mass conservation equation. The $\partial\rho/\partial t$ term in the continuity equation is substituted by the equivalent $\partial(\xi P)/\partial t$, where $\xi = \rho/P$ is calculated from the fluid mixture equation of state. This modification improves the convergence, especially for cases where buoyancy forces are significant. The final pressure Poisson equation is formed using the discretisation equations for the velocity components.

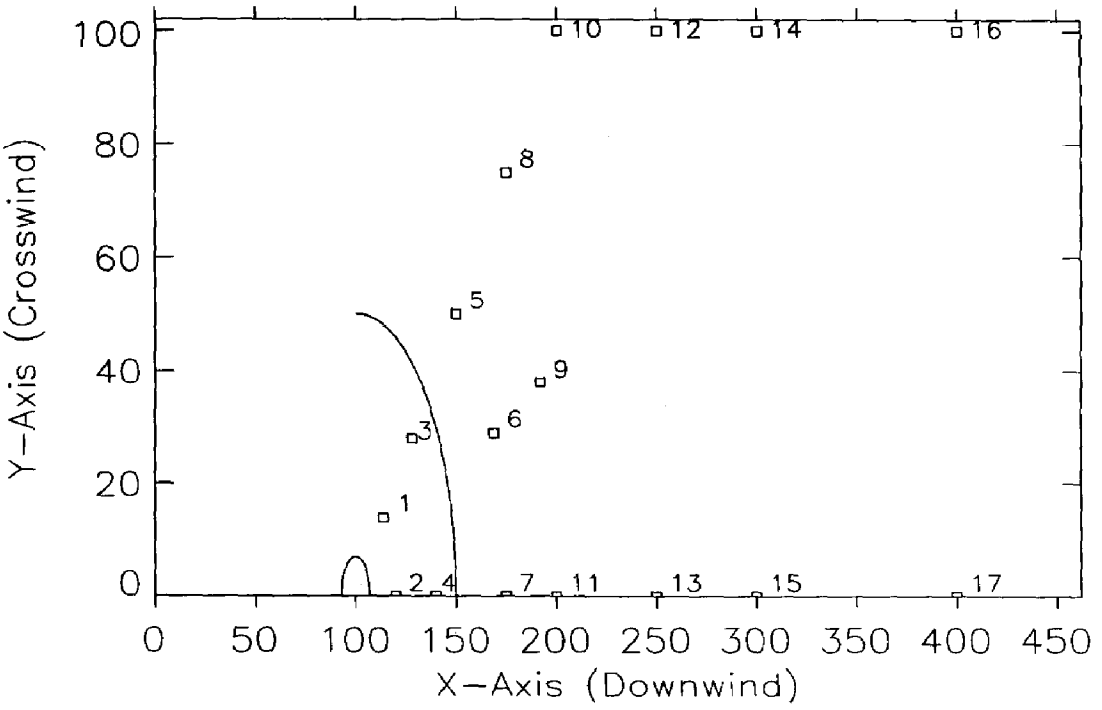

Fig. 1. Horizontal plan of computational domain, indicating the initial position of the gas cloud, the fence and the sensor positions.

2.5. *The computational domain for Thorney Island Trial 21*

Owing to the limitations in computer time and storage, it is assumed that the dispersion of the cloud is symmetrical about the wind direction. Therefore, the computational domain considered represents half of the real space affected by the released gas. This assumption is not far from reality, since the mean wind direction during experiment 21 deviated only by 6.1° from the plane of symmetry of the semi-circular fence. The experimental data (concentration versus time) for sensors located in symmetric positions with respect to the plane of symmetry are also very similar, which supports the assumption of symmetry in the dispersion. The only sensors for which this symmetry assumption is not valid are those found at the edges of the cloud during the dispersion.

The computational domain has the form of a rectangular box with the x-axis coinciding with the mean wind direction, the z-axis vertical to the ground and the y-axis perpendicular to the mean wind direction. The first ($J = 1$) xz-plane crosses the cylindrical source at the middle, i.e. it is the plane of symmetry. Fig. 1 is a horizontal plane of the domain, where the gas source, the fence and the sensor positions (numbered) are indicated.

The dimensions of the computational domain chosen are the following:

- x-axis (downwind), $x_{tot} = 463$ m;
- y-axis (crosswind), $y_{tot} = 102$ m;

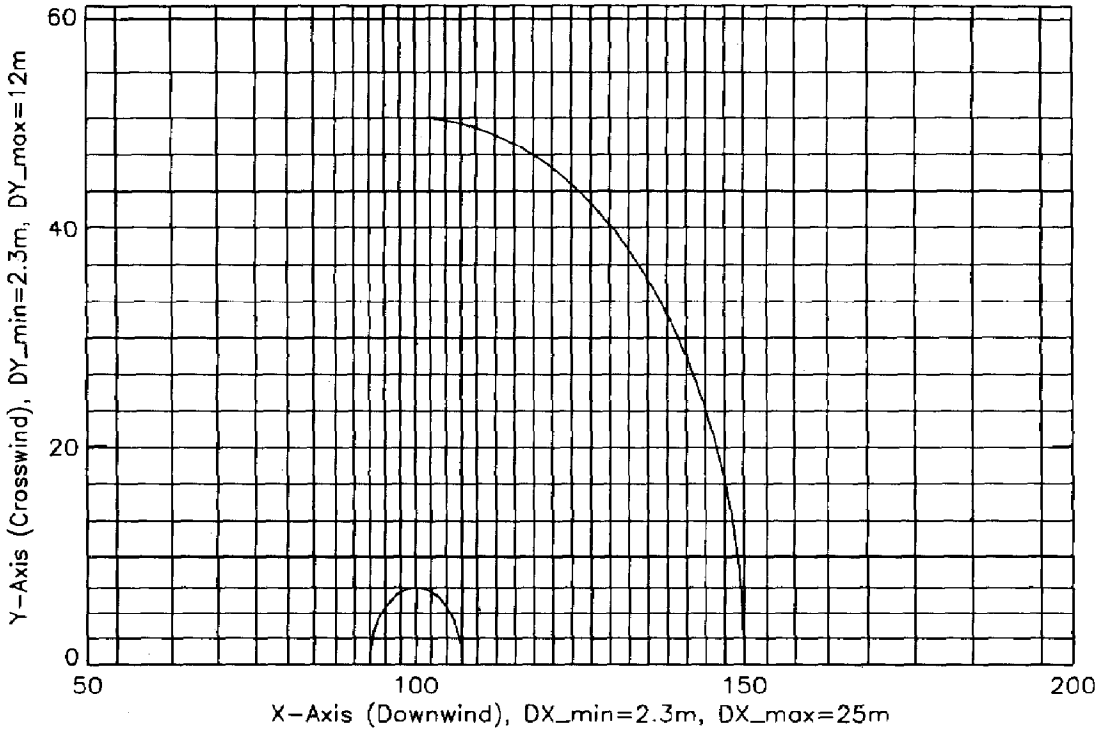

Fig. 2. Part of the horizontal (xy) grid, with the gas source and the fence indicated.

- z-axis (height), $z_{tot} = 36.5$ m.

The dimensions of the fence are

- radius, 50 m;
- height, 5 m.

The dimensions of the initial cylindrical gas cloud (source) are

- diameter, 14 m;
- height, 13 m.

The source centre (which coincides with the centre of the fence) was positioned approximately 100 m downwind of the inlet boundary surface.

The domain is discretised with a rectangular grid of

$$52\,(x\text{-axis}) \times 23\,(y\text{-axis}) \times 23\,(z\text{-axis}) = 27508 \text{ cells.}$$

The grid is not uniform since it is denser close to the source, between the source and the fence and close to the ground. The smallest cell is 2.3 m long in the x- and y-directions and 0.5 m in the z-direction. For reasons of clarity a part of the horizontal xy-grid with the position of the gas source and the fence is shown in Fig. 2.

3. Treatment of the semi-circular fence

As already mentioned, ADREA-HF is a finite volume code that uses a Cartesian coordinate system with rectangular cells. The fence used in Trial 21 of the Thorney

Island HGDT was semi-circular and very thin in comparison to the dimensions of the trial site and to the dimensions of our computational domain (see Fig. 1). This has two consequences.

(1) It is inevitable that, during the discretization of the domain, some cells are crossed by the fence (see Fig. 2).
(2) The horizontal discretisation close to the fence should be very fine to take into account correctly the very thin fence.

Some possible approximations of the fence of Trial 21 would be a fence consisting of straight parts following the cell interfaces, or a thick fence occupying the volume of a few cells. In these cases, however, a fine discretisation would again be necessary in order to approach the real dimensions of the fence (length, width and area).

The main interest of this study lies with the modelling of the *overall* effect of the *actual semi-circular, thin fence* on the flow field and the gas dispersion, while at the same time using a horizontal discretisation as coarse as possible (for reasons of economy in computer memory and execution time). In this respect, the following technique was adopted.

(1) The fence is considered to be infinitely thin, in the sense that it does not occupy any volume of the computational cells that it crosses. The fence consists only of two vertical solid boundary surfaces, each one facing the opposite direction to the other. The area of each of these surfaces equals the real area of the fence of Trial 21.
(2) The computational cells that are crossed by the fence were split into the following two categories:
   (a) *Blocked cells* in the x- or y- or both directions. If the centre of the cell was obstructed by the fence in the x- or y- direction, i.e. if in the particular cell that is crossed by the fence we draw a straight line passing from the cell's centre and parallel to the x- or y-axis and this line meets the fence inside this cell, then this cell is blocked in the x- or y-direction.
   (b) *Partially blocked cells* in the x- or y- or both directions, if the cell is crossed by the fence but is not blocked.
(3) In the blocked cells, no fluid should be passing between the two parts of the cell that are separated by the fence. Thus, at the middle-plane of these cells both horizontal convection and horizontal diffusion were put to zero in the transport equations for the total mass, momentum and dense gas mass (in the x-direction if the cell is x-blocked, in the y-direction if the cell is y-blocked or in both directions if it is blocked in both). The justification for this choice is that the middle plane of the cells coincides with the interface of the flow field cells, since the staggered grid methodology is adopted for the latter.
(4) For the partially blocked cells, the fence should not completely obstruct the flow, but act as a resistance to the flow. Thus, the part of the fence that belongs to a partially blocked cell was projected at the cell's middle planes (in the x- and y-directions). Then a flow *resistance coefficient* in the x- and y- directions was calculated as a function of the projection of the fence on the cell's middle planes. This resistance coefficient was calculated after the following empirical equation, proposed by Idelchik [12], for the case of a flow through a sharp-edged orifice in

a straight tube

$$\zeta_i \equiv \frac{\Delta P}{\rho u^2/2} = \left(1 + 0.707\sqrt{1 - \frac{A_{0,i}}{A_{1,i}}} - \frac{A_{0,i}}{A_{1,i}}\right)^2 \left(\frac{A_{1,i}}{A_{0,i}}\right)^2 \quad (6)$$

where ΔP is the pressure drop, ρ is the fluid density, u is the undisturbed velocity of the flow, $A_{1,i}$ is the undisturbed flow area in the i-direction (the cell's total vertical cross-section in our case) and $A_{0,i}$ ($A_{0,i} < A_{1,i}$) is the restricted flow area in the i-direction (the vertical cross-section of the cell left free if the fence projection is subtracted from the total cross-section). Eq. (6) was the most appropriate formula found in the literature that could be applied to the present case. The resistance coefficient increases abruptly as $A_{0,i}$ is decreased, so the transition from a partially blocked to a blocked cell is continuous. The implementation of the resistance coefficient ζ_i can be seen in the momentum equation shown in the Appendix.

Following the above-described approach we have one x-blocked cell in each horizontal line of cells parallel to the x-axis and one y-blocked cell in each horizontal line of cells parallel to the y-axis.

It should be noted that blocked and partially blocked cells have different qualitative behaviour, since in the latter fluid can pass from one part of the cell to the other.

The above method is not expected to reproduce the details of the flow very close to the obstacle. The justification of its use lies in how well it reproduces the global effect of the fence, which is the main point of interest.

4. Simulation of Thorney Island Trial No. 21

4.1. Input data relative to the experiment

The gas used in all the Thorney Island trials was a mixture of Freon-12 (CCl_2F_2) and nitrogen (N_2). The characteristics of the gas for Trial no. 21 were the following:

- initial relative density (to air), $\rho_r = 2.02$ ($\pm 4\%$);
- released volume, 2050 m^3 ($\pm 5\%$);
- isothermal (ambient temperature).

The atmospheric stability conditions were assessed to be *neutral*. The average wind velocity at 10 m height was 3.9 m/s (± 0.1 m/s) and the ambient air temperature was 20.9 °C (± 0.2 °C).

4.2. Calculation of the wind velocity profile

The first computational step was to calculate the undisturbed wind velocity profile for the particular trial. This was done by solving the momentum conservation equation in one dimension, i.e. only diffusion along the z-direction. A pressure gradient $dP/dx = -1.4 \times 10^{-3}$ Pa/m was also adopted as the driving force of the flow, in order to have at 10 m height a wind speed of 3.9 m/s, which is the given

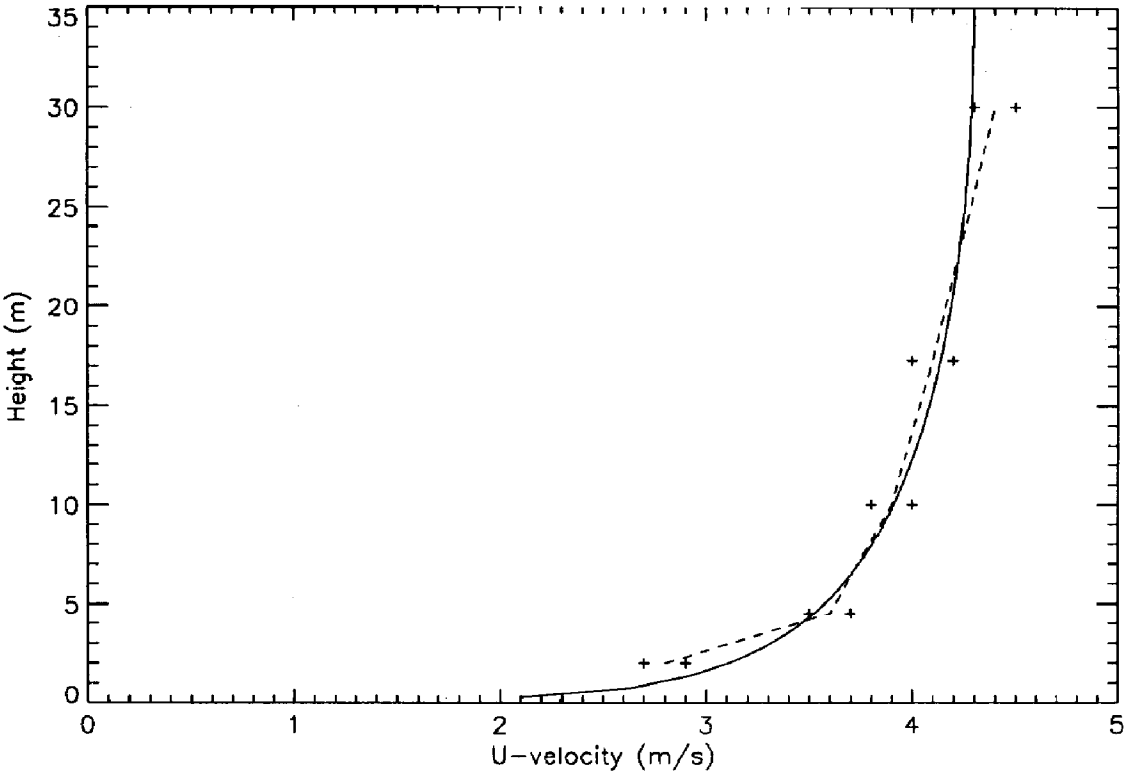

Fig. 3. (——) Calculated and (– – –) experimental undisturbed wind velocity profiles.

experimental value. The calculated and the experimentally obtained wind velocity profiles are shown in Fig. 3.

4.3. Calculation of the steady-state wind field

The second step was the computation of the steady-state wind field, formed around the solid cylindrical gas container and around the semi-circular fence, prior to the gas release. This step was achieved using as input the already obtained wind profile and solving the total mass and momentum conservation equations, in three-dimensional form, until a steady state was reached. A plot of the calculated velocity vector field on the vertical xz-plane ($J = 1$, i.e. the plane of symmetry) is given in Fig. 4. The calculated velocity vector field on the horizontal xy-plane ($K = 1$, i.e. the ground plane) is shown in Fig. 5. This step was performed because the wind field in which the cloud is released affects its advection as well as its dilution rate. Furthermore, the dynamical pressure distribution around the cylindrical container is important for the initial phases of the dilution of the cloud.

4.4. Transient calculation of the cloud dispersion

Using the velocity, pressure and turbulent kinetic energy distributions from the previous step as initial conditions, the transient calculation of the gas dispersion was

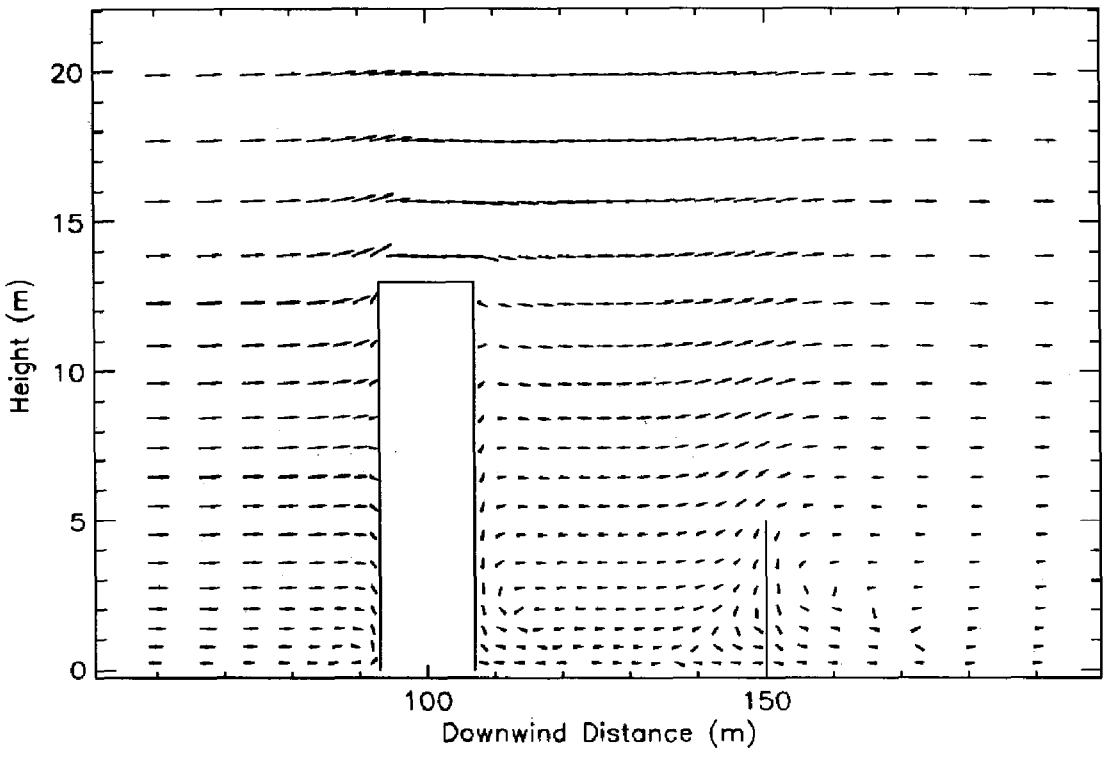

Fig. 4. Calculated steady-state wind velocity field, before the gas release, at the vertical (symmetry) plane. The scaling of the velocities is different for the two axes.

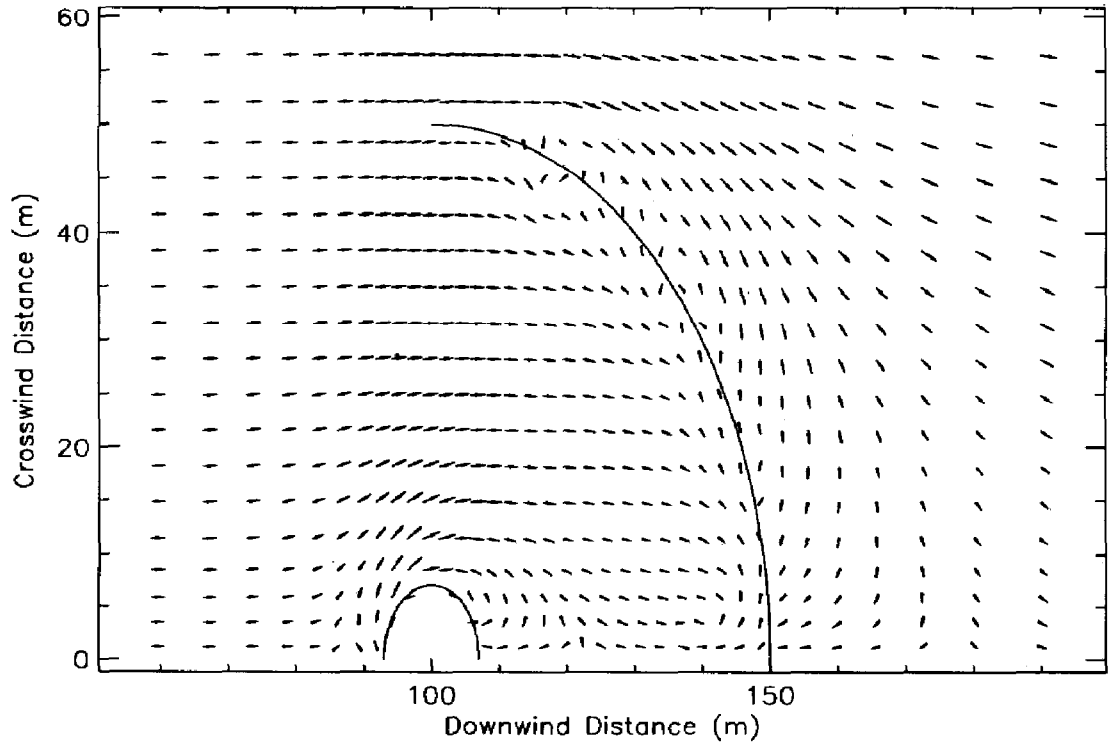

Fig. 5. Calculated steady-state wind velocity field, at the horizontal (ground) plane. The scaling of the velocities is different for the two axes.

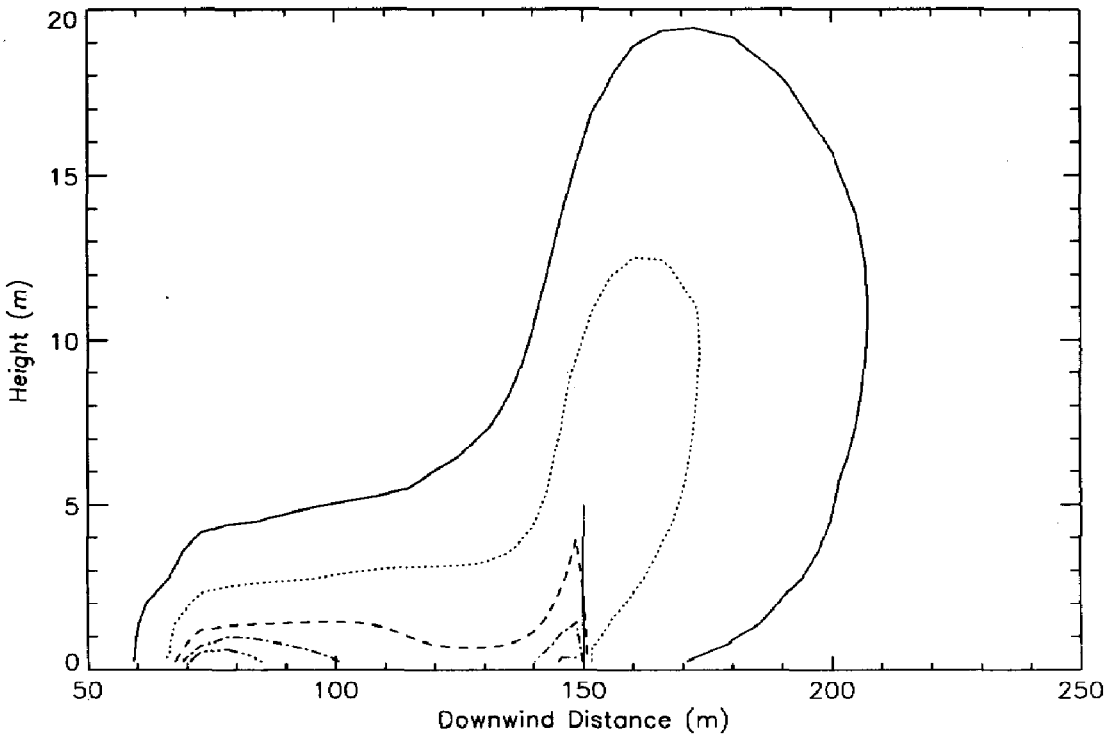

Fig. 6. Contour plot of dense gas mass fraction at the vertical (symmetry) plane at time 30 s after the release. (—) 0.001; (- - -) 0.010; (– – –) 0.050; (– – – –) 0.100; (– – – – –) 0.150.

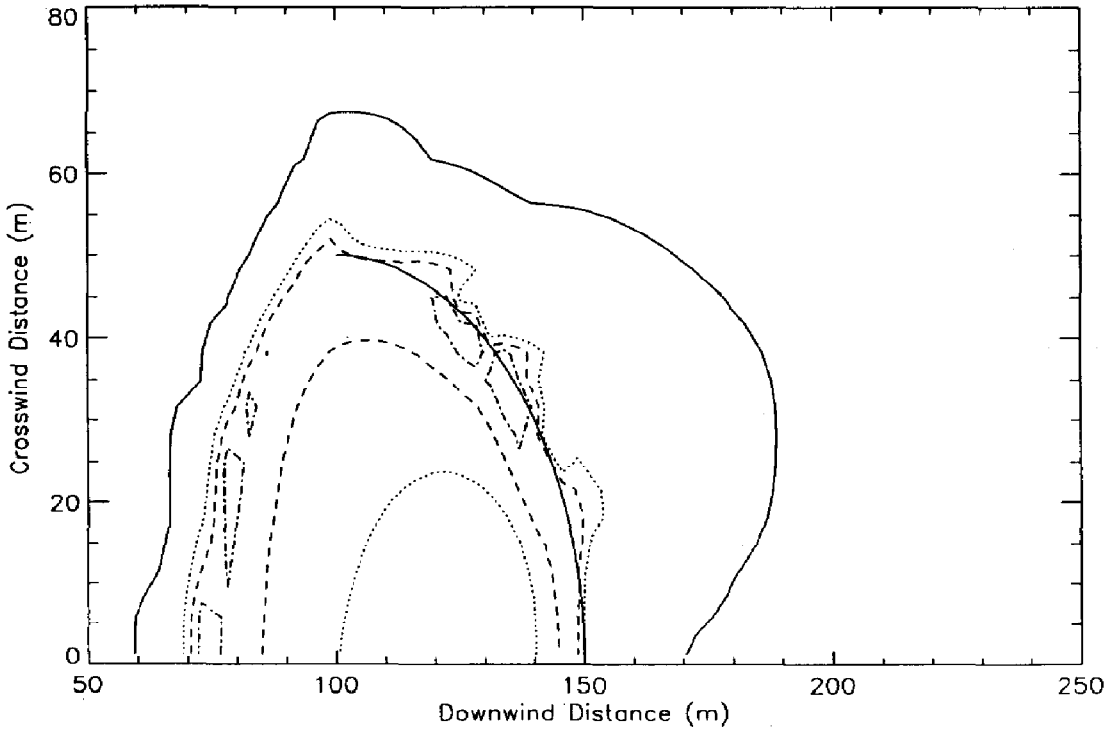

Fig. 7. Contour plot of dense gas mass fraction at the horizontal (ground) plane at time 30 s after the release. (—) 0.001; (- - -) 0.100; (– – –) 0.150; (– – – – –) 0.200.

performed as the final stage. In this step the three conservation equations for the total mass, momentum and dense gas mass were solved. The computations started at 0.0 s, with a still, dense gas column standing in the place of the container and continued until 500.0 s, when the cloud centre had drifted out of the domain.

Fig. 6 shows the contour plot of the calculated gas mass fraction at the 30th second after the release for the vertical plane of symmetry and Fig. 7 shows the corresponding plot for the horizontal plane at the ground.

Fig. 8(a) shows the calculated velocity field at 10 s after the release, when the cloud has not yet reached the fence, for the horizontal plane at the ground. Fig. 8(b) is the corresponding velocity field at 50 s after the release.

4.5. Comparison with the experimental data

For comparison purposes, the computed concentration values at all grid points of the computational domain were interpolated to determine the corresponding values at the positions of the sensors. The calculated and the measured concentration–time histories were plotted together and compared (see Figs. 9–13). The comparison concerns the shape of the curves, the maximum concentration and the cloud arrival and departure times. Two positions inside the fence (Figs. 9(a) and (b) and 10(a)–(c)) and three positions outside the fence (Figs. 11(a) and (b), 12(a) and (b) and 13(a) and (b)) are included. Except for Fig. 10(c), comparisons for elevations greater than 2.4 m have not been included, since the experimental data at those heights present significant fluctuations and it is therefore difficult to draw any conclusions.

5. Discussion and conclusions

The first point that is worth noting is the good agreement between the wind velocity profiles, shown in Fig. 3. It indicates that the adopted turbulence model performs well also in the absence of a dense gas, for neutral ambient conditions. The correct computation of the wind velocity is also important for the correct prediction of the advection speed of the gas cloud.

The vector plots in Figs. 4 and 5 give a qualitative picture of the predicted steady-state wind velocity field, before the release of the gas. The calculated flow patterns around the cylindrical container and the fence are quite reasonable and characteristic recirculation zones are predicted in the wake of these bodies.

The contour plots of the gas mass fraction (Figs. 6 and 7) show that the adopted modelling approach for the fence reproduces most of the real effects of the obstacle on the dispersion of the cloud, as described in [6]. From the horizontal contour plot (Fig. 7), it is apparent that the cloud has been held up in the fenced area: higher concentrations exist upwind of the fence than downwind, where the dilution of the cloud is much faster. The vertical contour plot (Fig. 6) shows that the cloud front "splashes" over the fence and is raised up to three times the height of the fence. These phenomena were also reported during the experimental campaign.

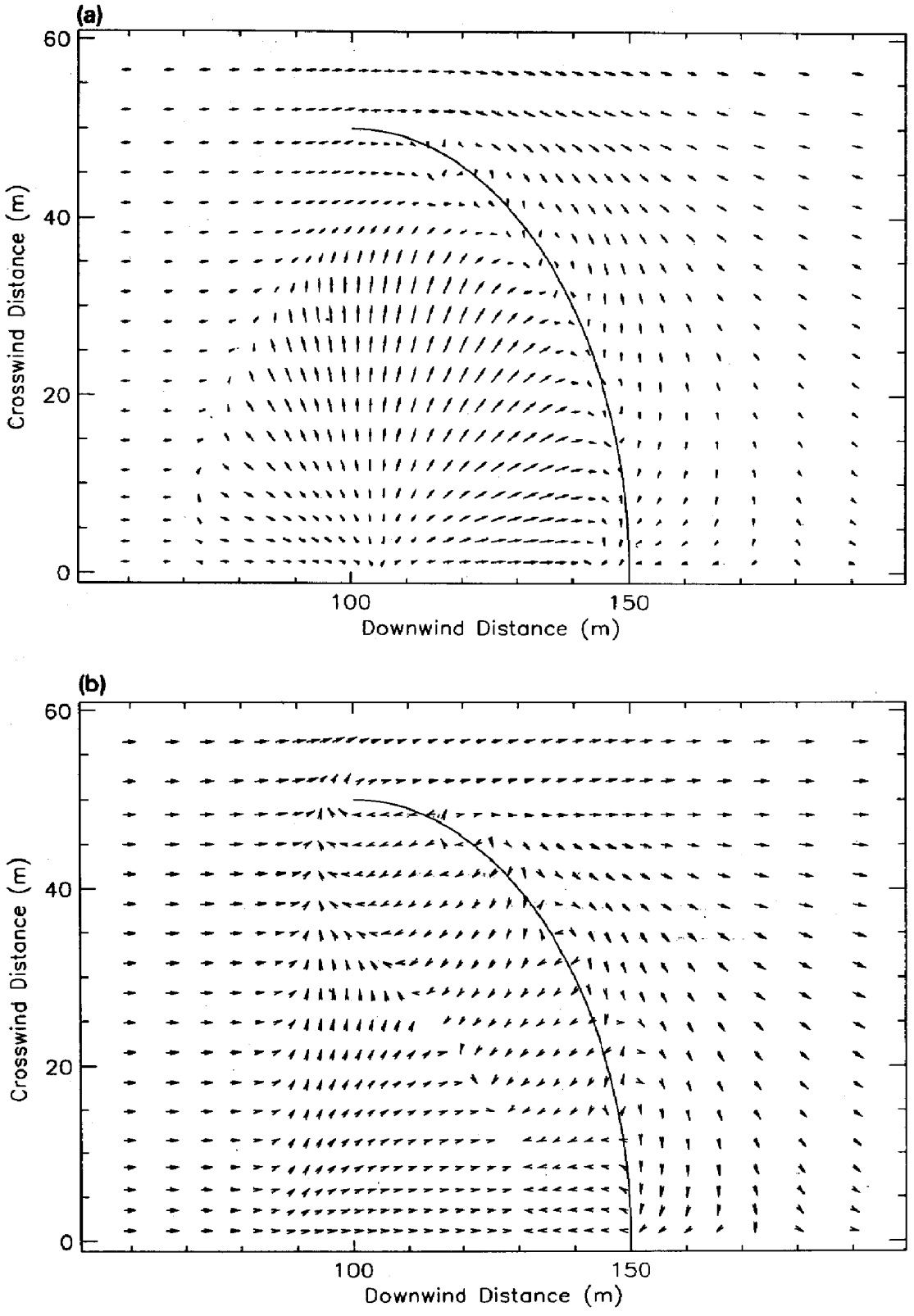

Fig. 8. Velocity vector plots at the horizontal (ground) plane at times: (a) 10 s and (b) 50 s, after the release.

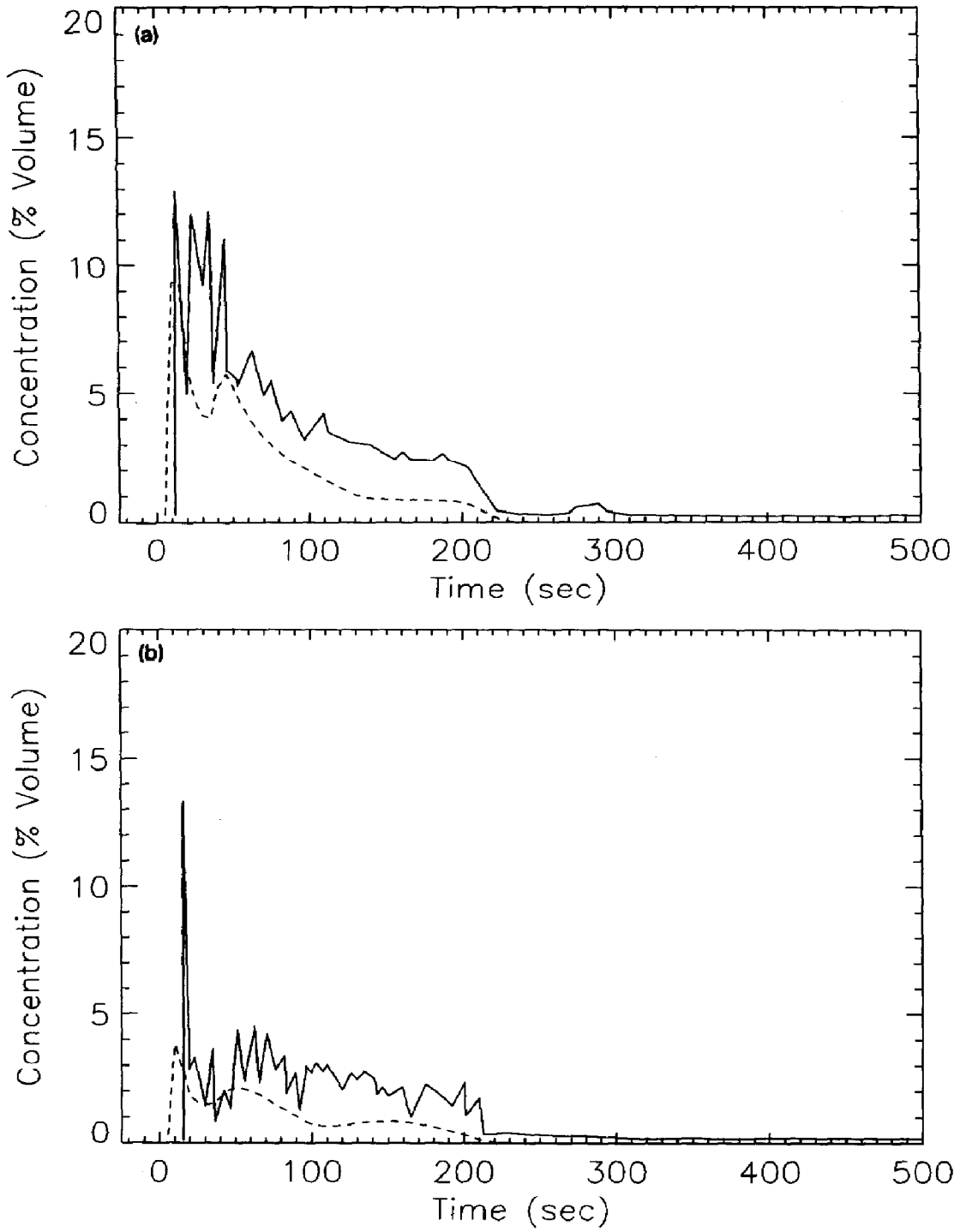

Fig. 9. Concentration versus time for sensor No. 3 (see Fig. 1), for heights: (a) 0.4 m and (b) 2.4 m. (—) Experiment; (– – –) ADREA-HF.

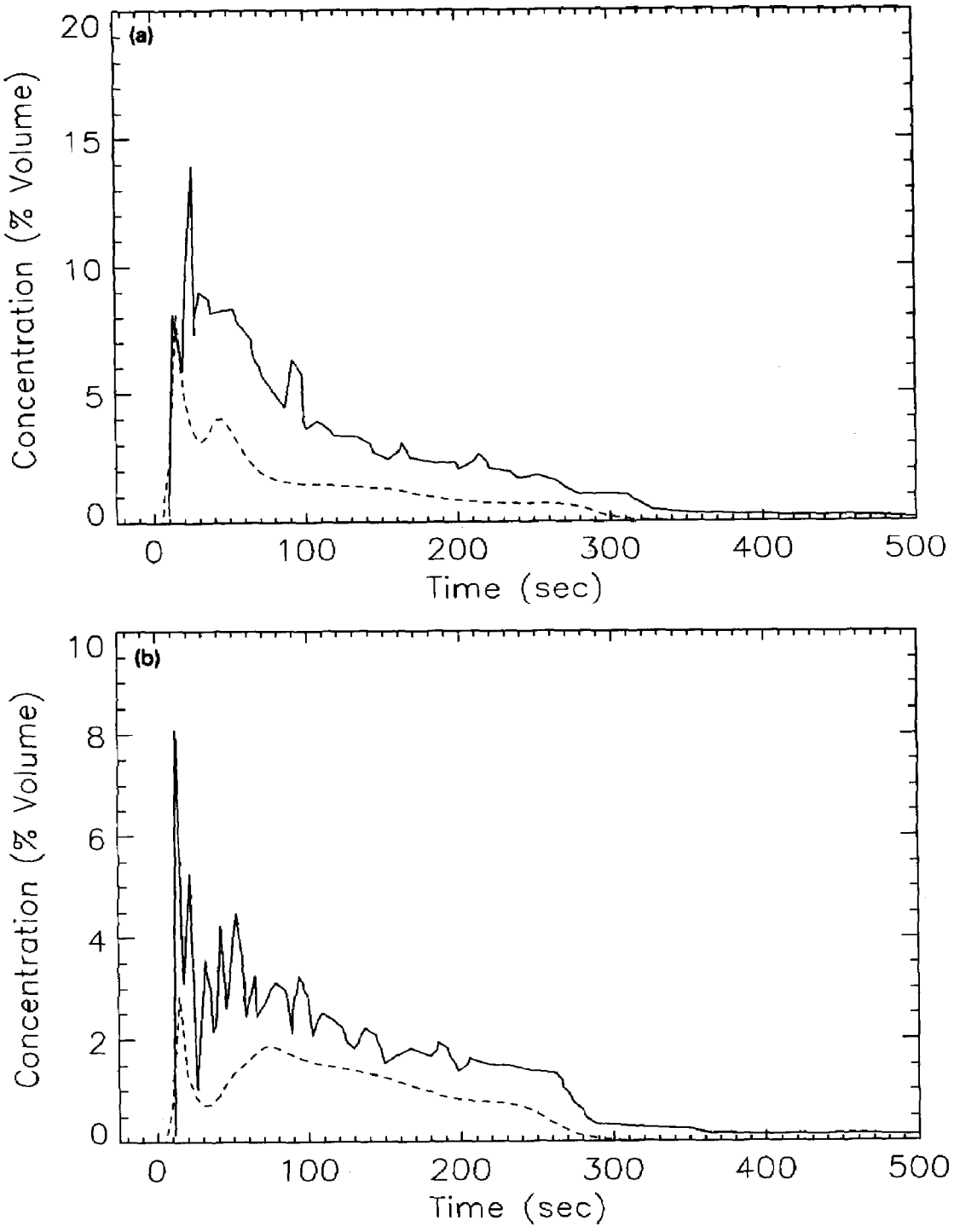

Fig. 10. Concentration versus time for sensor No. 4 (see Fig. 1), for heights: (a) 0.4 m and (b) 2.4 m and (c) 4.4 m. (—) Experiment; (– – –) ADREA-HF.

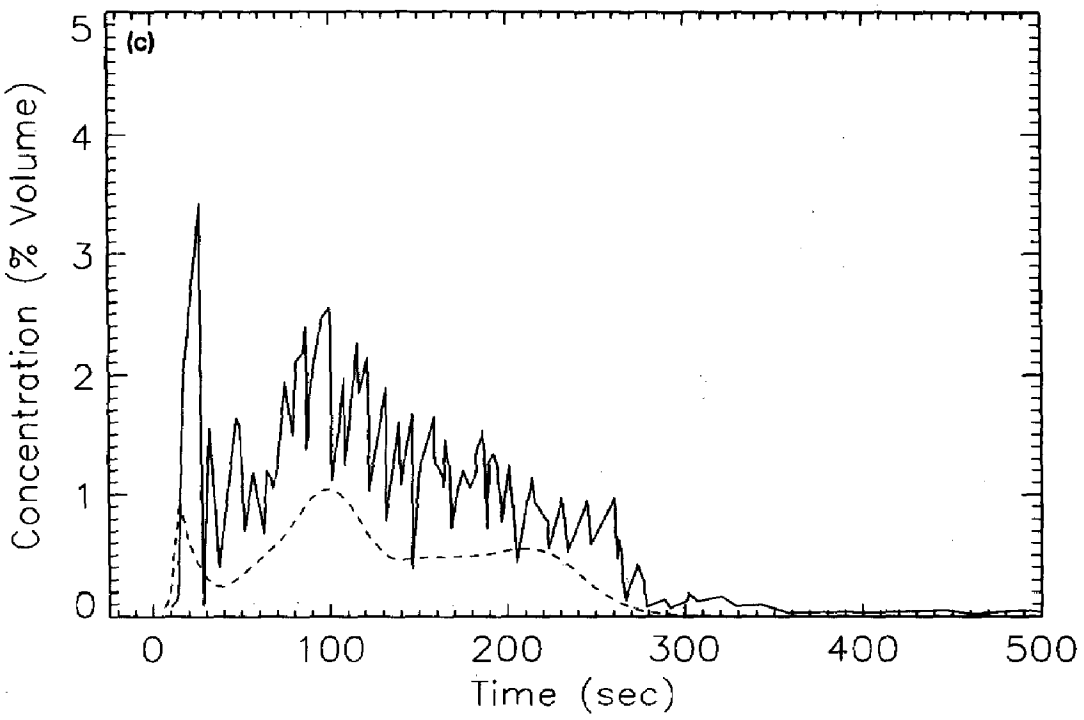

Fig. 10. (continued)

The interaction between the cloud and the obstacle is also seen in the velocity vector plots in the horizontal plane at the ground (see Figs. 8(a) and (b)). The cloud spreads radially (Fig. 8(a)), until it reaches the fence on which it is "reflected" and then it starts moving backwards (Fig. 8(b)).

This motion of the cloud, due to the obstacle, is also demonstrated by Figs. 9(a) and (b) and 10(a)–(c), which present characteristic cases of the concentration–time histories for positions inside the fence (refer to Fig. 1 for the numbering of the sensors). In these curves, two concentration peaks are observed. The second peak is due to the return flow following the cloud splashing on the fence. The calculated curves follow the same pattern and predict quite satisfactorily the cloud arrival and departure times.

Figs. 11(a) and (b), 12(a) and (b) and 13(a) and (b) refer to positions outside the fence. Therefore, there is only one concentration peak and the level of the concentration is much lower than inside the fence. Here again, the model predictions are quite satisfactory. The overall shape and the timing (arrival and departure times) of the calculated curves agree well with the experimental ones.

In conclusion, the combination of the flow resistance coefficient with the blocked cells gives the expected flow patterns around the obstacle. From the above presented comparison between the experimental and the calculated curves of concentration versus time, we also conclude that the present modelling approach predicts rather successfully the overall effects of the obstacle on dense gas dispersion.

Nevertheless, the model has a tendency to underestimate the dense gas maximum concentration. This is clearly shown in Fig. 14 where the calculated peak

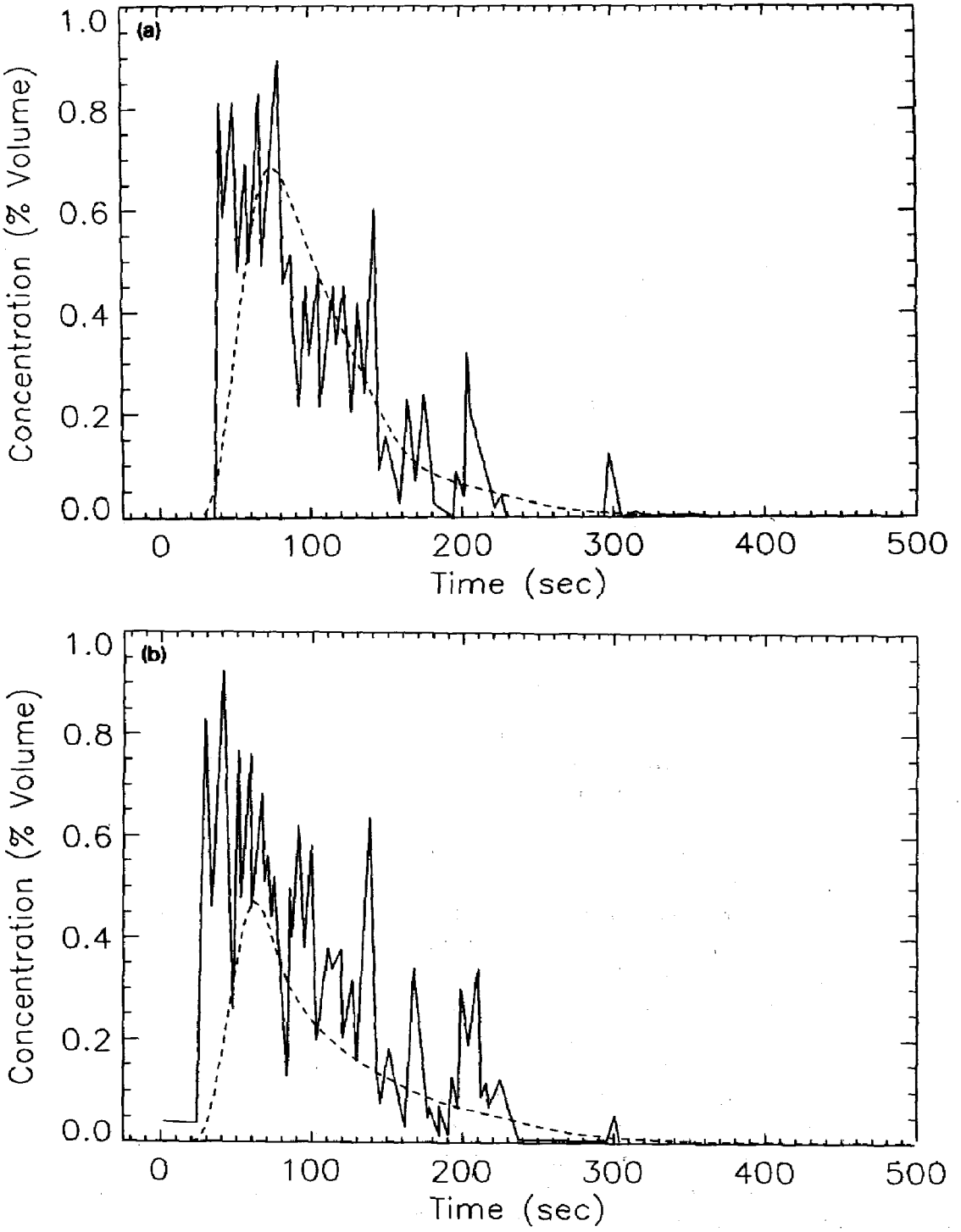

Fig. 11. Concentration versus time for sensor No. 9 (see Fig. 1), for heights: (a) 0.4 m and (b) 2.4 m. (—) Experiment; (– – –) ADREA-HF.

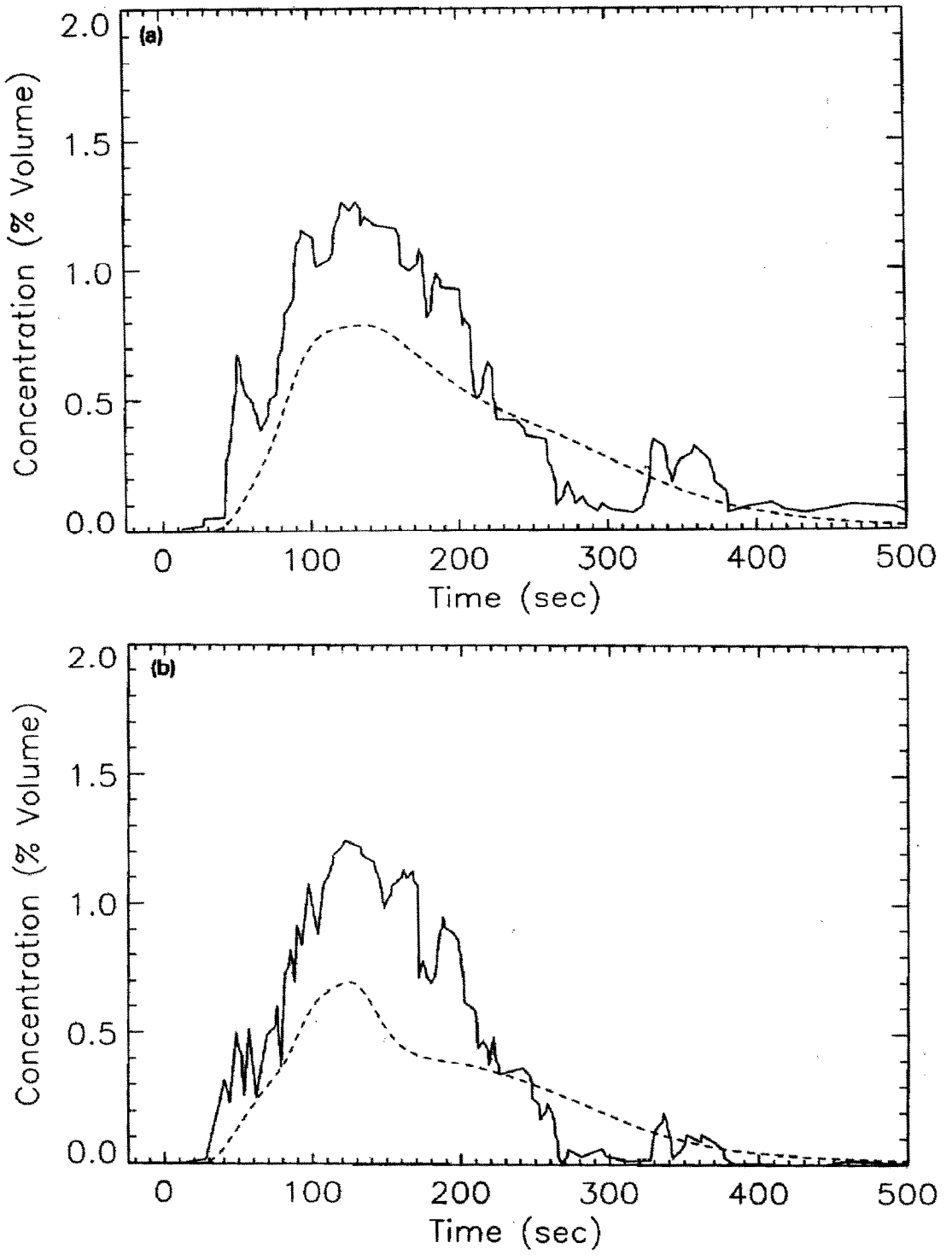

Fig. 12. Concentration versus time for sensor No. 11 (see Fig. 1), for heights: (a) 0.4 m and (b) 2.4 m. (—) Experiment; (– – –) ADREA-HF.

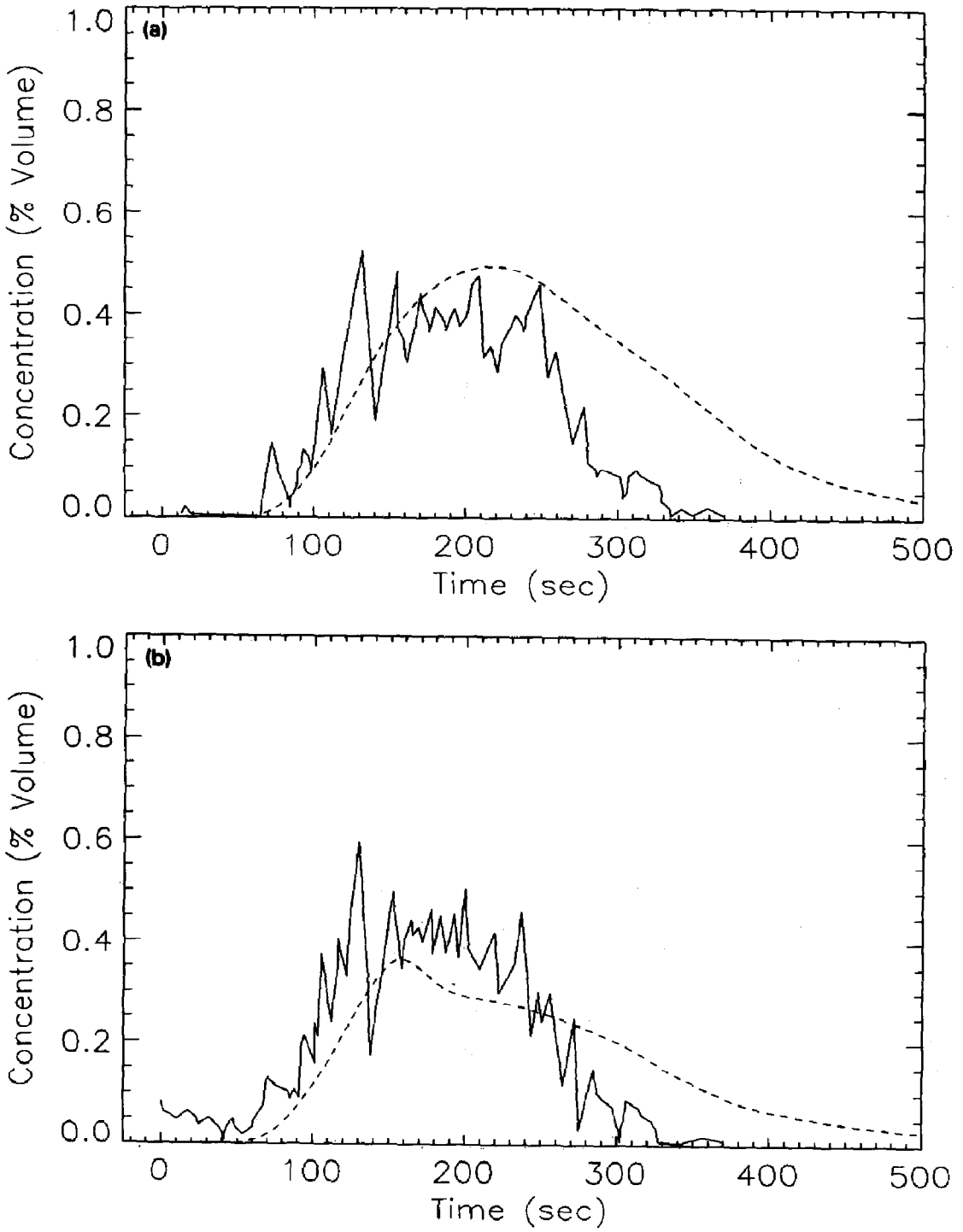

Fig. 13. Concentration versus time for sensor No. 15 (see Fig. 1), for heights: (a) 0.4 m and (b) 2.4 m. (—) Experiment; (– – –) ADREA-HF.

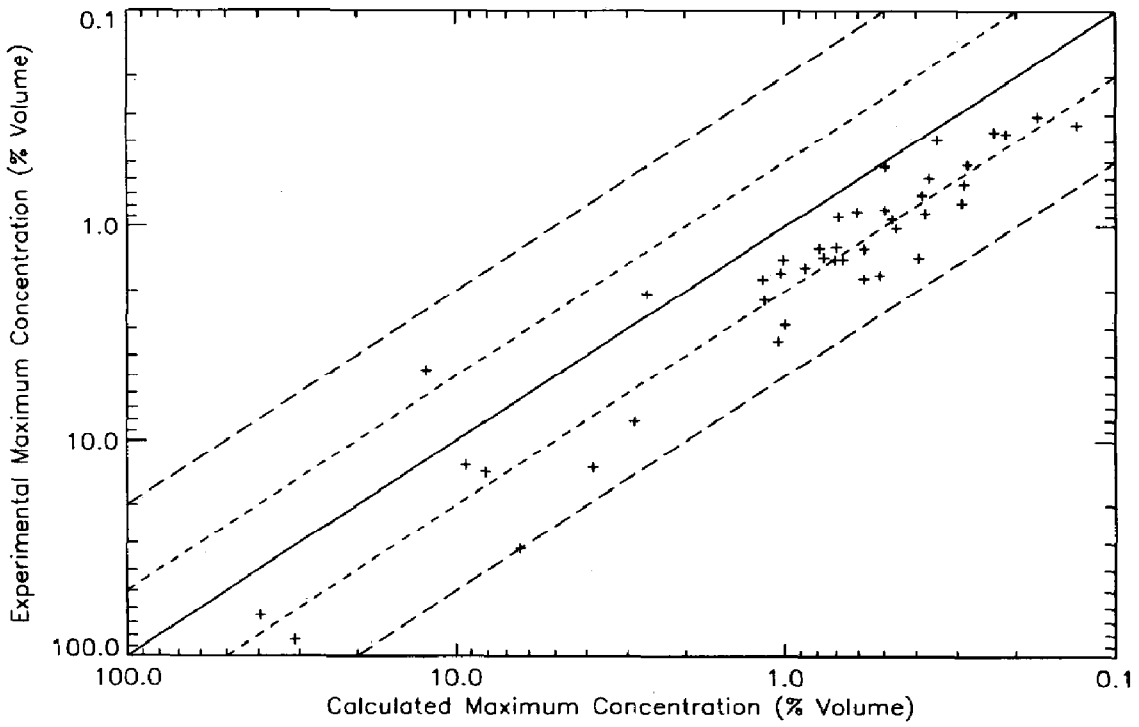

Fig. 14. Experimental versus calculated maximum concentrations (the axes are scaled in descending order). (—) Calc./exper. = 1; (- - -) calc./exper. = 2 or 1/2; (— — —) calc./exper. = 5 or 1/5.

concentrations are compared with the experimental ones. This figure was drawn, following the recommendations of Ermak and Merry [13] (note that the axes are scaled in descending order). In drawing Fig. 14 we did not take into account the sensors with numbers 8, 10, 12, 14, 16 (see Fig. 1), because of the assumption of symmetrical dispersion which is not valid for these sensors (as already mentioned and as seen from the experimental data). In fact the corresponding sensors at the symmetrically opposite positions (with respect to the x-axis of our domain) did not detect gas during the experiment. This is due to the fact that the mean wind direction during the experiment did not coincide with the centre line of the trial site but was 6.1° off to the left.

In Fig. 14 we observe that nearly all the points are located lower than the "calculated = experimental" line and around the "calculated/experimental = 1/2" line. Thus, on average, the predicted maximum concentration will be half of the experimentally observed value. This is partly explained by the fact that a model like the one used here calculates average values of concentration and in this respect it cannot predict the high peaks of short duration which were observed during the experiment.

A better basis of comparison is therefore to calculate the doses (defined as integral of the concentration with time for the duration of the calculation, i.e. 500 s). Fig. 15 presents the comparison between experimental and predicted doses for the same sensor positions as in Fig. 14. Here again it is clear that the model tends to

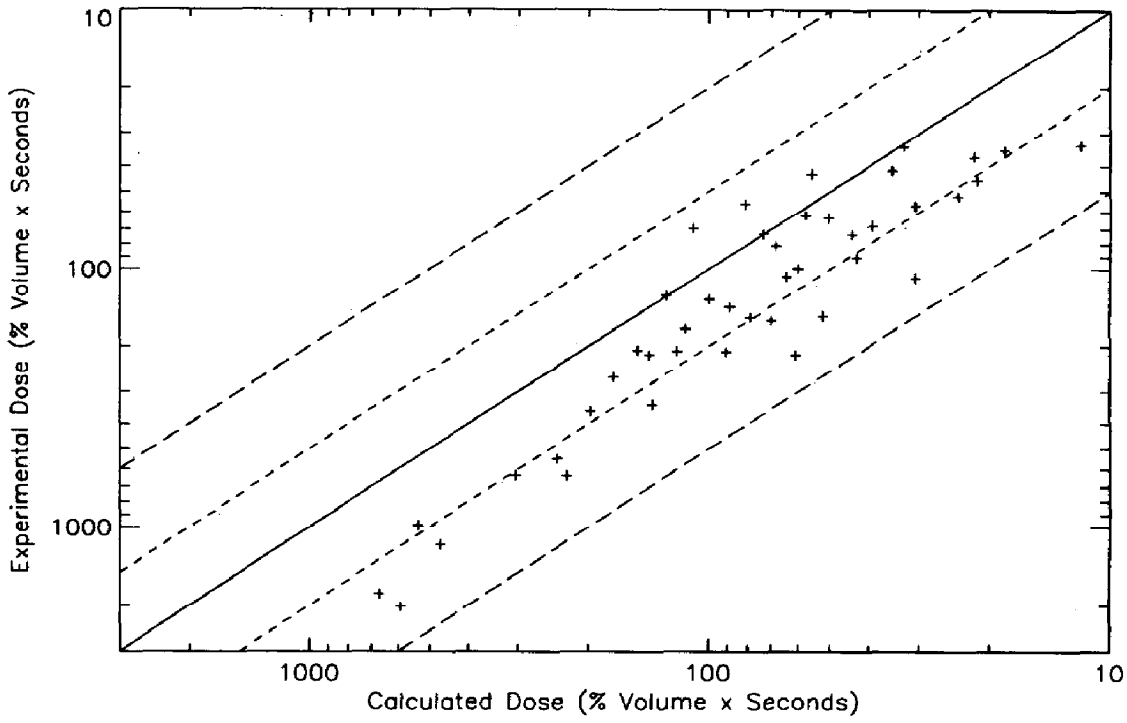

Fig. 15. Experimental versus calculated doses (the axes are scaled in descending order). (—) Calc./exper. = 1; (- - -) calc./exper. = 2 or 1/2; (– – –) calc./exper. = 5 or 1/5.

underestimate the dose but to a lesser extent than the maximum concentration, since now more points are close to the "calculated = experimental" line.

The main conclusion that can be drawn from the above is that the adopted model has the tendency to underestimate the concentration of the dense gas. A possible cause for this is the turbulence modelling, which might underestimate the damping effect of the strongly stable density stratification upon the eddy mass diffusivity, i.e. upon the mixing of the gas with the ambient air.

On the other hand, our model predicts only average values of concentration, while the experimental data strongly fluctuate. Thus, it is necessary to include in the model the calculation of concentration fluctuations in addition to the concentration mean values. In this way, we could evaluate the confidence intervals for the model predictions and judge whether the model actually underestimates the concentration, or if it is just the statistical nature of the experimental data that causes these differences between the calculated and the measured data.

6. Nomenclature

c_p specific heat under constant pressure (J/kg K)
c_v specific heat under constant volume (J/kg K)
C_D, C_N turbulence model constants (dimensionless)

C_μ, C_Γ turbulence model constants (dimensionless)
g_n gravity acceleration component in the $\hat{n}$-direction (m/s^2)
I cell number along the x-direction (dimensionless)
J cell number along the y-direction (dimensionless)
k turbulent kinetic energy (per unit mass) (m^2/s^2)
K cell number along the z-direction (dimensionless)
K_{mi} turbulent momentum diffusivity in the i-direction ($i = x, y, z$) (m^2/s)
K_{mn} turbulent momentum diffusivity in the $\hat{n}$-direction (m^2/s)
$K_{\omega i}$ turbulent mass diffusivity in the i-direction ($i = x, y, z$) (m^2/s)
l_{gn} wall length scale of turbulence in the $\hat{n}$-direction (m)
l_n effective length scale of turbulence in the $\hat{n}$-direction (m)
l_{sn} stability length scale of turbulence in the $\hat{n}$-direction (m)
l_0 global pressure field length scale of turbulence (m)
$\hat{n}$ unit vector normal to a surface of arbitrary orientation (dimensionless)
N_n Brunt–Väisälä frequency in the $\hat{n}$-direction (s^{-1})
P pressure (N/m^2)
Ri gradient Richardson number (dimensionless)
Ri_f flux Richardson number (dimensionless)
Ri_{fc} critical flux Richardson number (dimensionless)
t time (s)
x distance along x-axis (downwind) (m)
x_{tot} dimension of computational domain in the x-direction (m)
y distance along the y-axis (crosswind) (m)
y_{tot} dimension of computational domain in the y-direction (m)
z distance along the z-axis (height) (m)
z_{tot} dimension of computational domain in the z-direction (m)
Γ asymptotic pressure field acceleration (m/s^2)
ζ flow resistance coefficient (dimensionless)
λ molecular conductivity (J/m s K)
μ molecular viscosity (kg/m s)
ρ density (kg/m s)
σ_h turbulent Prandtl number (dimensionless)

7. Appendix

7.1. The transport equations

The set of conservation equations solved by ADREA-HF, for the simulation of Thorney Island Trial 21 (single phase, isothermal case) is the following:

Total mass

$$\frac{\partial \rho}{\partial t} + \frac{\partial}{\partial x_i}(\rho u_i) = 0 \tag{A.1}$$

Momentum

$$\frac{\partial}{\partial t}(\rho u_i) + \frac{\partial}{\partial x_j}(\rho u_i u_j) = -\frac{\partial P}{\partial x_i} + \frac{\partial}{\partial x_j}\left(\rho K_{mj}\frac{\partial u_i}{\partial x_j}\right) + \rho g_i - Z_i \tag{A.2}$$

Mass of dense gas

$$\frac{\partial}{\partial t}(\rho\omega) + \frac{\partial}{\partial x_i}(\rho u_i \omega) = \frac{\partial}{\partial x_i}\left(\rho\frac{K_{mi}}{\sigma_h}\frac{\partial\omega}{\partial x_i}\right) \tag{A.3}$$

where ρ is the mixture (air–dense gas) density, u_i is the velocity in the i-direction ($i = x, y, z$), P is the pressure, K_{mi} is the eddy viscosity in the i-direction, g_i is the gravity acceleration in the i-direction, Z_i is the distributed resistance of the flow in the i-direction, ω is the dense gas mass fraction and σ_h is the turbulent Prandtl number. The resistance is given by

$$Z_i = -\frac{\zeta_i}{\delta x_i}\frac{\rho|u_i|u_i}{2} \tag{A.4}$$

where ζ_i is the resistance coefficient, given by Eq. (6) and δx_i is the horizontal grid resolution, both in the i-direction.

In the above equations the eddy viscosity–diffusivity approach is adopted to model the turbulent fluxes:

$$-\overline{u_i' u_j'} = K_{mj}\frac{\partial u_i}{\partial x_j} \tag{A.5a}$$

$$-\overline{u_i'\omega'} = \frac{K_{mi}}{\sigma_h}\frac{\partial\omega}{\partial x_i} \tag{A.5b}$$

7.2. The turbulent momentum diffusion coefficients

The eddy viscosity K_{mi} is calculated as follows [1, 2]:

$$K_{mi} = C_\mu k^{1/2} l_i \tag{A.6}$$

where k is the turbulent kinetic energy, l_i is the effective length scale in the i-direction and C_μ ($= 0.1887$) is an empirical constant.

The turbulent kinetic energy is computed by solving the following transport equation:

$$\frac{\partial}{\partial t}(\rho k) + \frac{\partial}{\partial x_i}(\rho u_i k) = \frac{\partial}{\partial x_i}\left(\rho\frac{K_{mi}}{\sigma_k}\frac{\partial k}{\partial x_i}\right) + G + G_B - \rho\varepsilon \tag{A.7}$$

Here $\sigma_k = 1.0$ is a constant, G and G_B are the mechanical and the buoyancy production (or dissipation) terms, respectively,

$$G = -\overline{\rho u_i' u_j'}\frac{\partial u_i}{\partial x_j}, \qquad G_B = \overline{\rho' u_i' g_i} \tag{A.8}$$

and ε is the viscous dissipation rate, modelled as

$$\varepsilon = C_D \frac{k^{3/2}}{l_*}, \quad C_D = 0.3 \tag{A.9}$$

where $l_* = \min(l_x, l_y, l_z)$. The ratio of the buoyancy production (or dissipation) rate to the mechanical production rate is defined as the flux Richardson number Ri_f; the latter is equal to the gradient Richardson number Ri divided by the turbulent Prandtl number σ_h:

$$Ri_f = -\frac{G_B}{G} = \frac{Ri}{\sigma_h} \tag{A.10}$$

Thus, Eq. (A.7) is written as follows:

$$\frac{\partial}{\partial t}(\rho k) + \frac{\partial}{\partial x_i}(\rho u_i k) = \frac{\partial}{\partial x_i}\left(\rho \frac{K_{mi}}{\sigma_k}\frac{\partial k}{\partial x_i}\right) + G\left(1 - \frac{Ri}{\sigma_h}\right) - \rho\varepsilon \tag{A.11}$$

The gradient Richardson number is defined, according to [1] as

$$Ri = g_i K_{mi}\left(\frac{1}{\rho}\frac{\partial \rho}{\partial x_i} - \frac{c_v}{c_p}\frac{\rho}{P}g_i\right)\frac{\rho}{G} \tag{A.12}$$

The effective length scale l_i, to be used in Eq. (A.6), is calculated from

$$\frac{1}{l_i} = \left[\left(\frac{1}{l_{gi}} + \frac{1}{l_{si}}\right)^n + \left(\frac{1}{l_0}\right)^n\right]^{1/n}, \quad n = 5 \tag{A.13}$$

where l_{gi} is a wall length scale, equal to the shortest distance of the particular point from a solid boundary in the i-direction, l_{si} is a stability length scale in the i-direction and l_0 is an "outer" length scale, given by the relations

$$l_{si} = C_N \frac{k^{1/2}}{N_i}$$

$$l_0 = C_\Gamma \frac{k}{\Gamma}$$

$$\Gamma = \frac{1}{\rho}\left[\sum_i \left(\frac{\partial P}{\partial x_i}\right)_\infty^2\right]^{1/2}$$

$$C_N = 0.51, \quad C_\Gamma = 0.49$$

where N_i is the Brunt–Väissälä frequency in the i-direction. The above model is based on the assumption that turbulence length scales mainly depend on the presence of ground, local stability conditions and the global pressure acceleration field (Γ).

According to [1], the Brunt–Väissälä frequency N_i is defined as

$$N_i = \left[g_i\left(\frac{1}{\rho}\frac{\partial \rho}{\partial x_i} - \frac{c_v}{c_p}\frac{\rho}{P}g_i\right)\right]^{1/2} \tag{A.14}$$

The eddy mass diffusivity, as can be seen in Eqs. (A.3) and (A.5b) is related to the eddy viscosity via the turbulence Prandtl number σ_h, which depends mainly on the flow stability. According to [1], for unstable flows, σ_h is given by

$$\sigma_h = Pr \frac{(1 - 9\,Ri)^{-1/2}}{(1 - 15\,Ri)^{-1/4}} \quad \text{for } Ri < 0 \tag{A.15}$$

while, for stable flows, as inside a dense gas cloud, σ_h is given by Eq. (5). Here Pr is the classical Prandtl number $Pr = \mu c_p/\lambda = 0.71$ and Ri_{fc} is the critical flux Richardson number, for which a value of 0.15 is assumed [9].

8. Acknowledgements

The authors would like to thank the Commission of the European Communities, Directorate General for Science, Research and Development, for partial support of this work, in the framework of the S.T.E.P. programme.

9. References

[1] J.G. Bartzis, ADREA-HF: a three-dimensional finite volume code for vapour cloud dispersion in complex terrain, Report EUR 13580 EN, 1991.
[2] J.G. Bartzis, Turbulent diffusion modelling for wind flow and dispersion analysis, Atmos. Environ., 23 (1989) 1963–1969.
[3] S. Andronopoulos, J.G. Bartzis, J. Würtz and D. Asimakopoulos, Simulation of the Thorney Island Dense Gas Trial No. 8, using the code ADREA-HF, Process Saf. Progr., 12 (1993) 61–66.
[4] B. Carissimo, S. Andronopoulos, J.G. Bartzis and J. Würtz, Intercomparison on heavy gas dispersion between the three-dimensional models MERCURE and ADREA. Part 1. Instantaneous release without obstacle, Report EDF HE-33/92-15, 1992.
[5] J.C. Statharas, J.G. Bartzis and J. Würtz, Prediction of ammonia releases using ADREA-HF code, presented at the 1992 AIChE Summer Meeting, Minneapolis, USA, August 9–12, 1992.
[6] J. McQuaid and B. Roebuck, Large scale field trials on dense vapour dispersion, Report EUR 10029 EN, 1985.
[7] P. Schreurs and J. Mewis, Development of a transport phenomena model for accidental releases of heavy gases in an industrial environment, Atmos. Environ., 21 (1987) 765–776.
[8] R.B. Lantz, K.H. Coats and C.V. Kloepfer, A three-dimensional numerical model for calculating the spread and dilution of air pollutants, in: Proc. Symp. on Air Pollution Turbulence and Diffusion, Las Cruces, NM, February 7–9, 1971.
[9] T.H. Ellison and J.S. Turner, Mixing of dense fluid in a turbulent pipe flow. Part 2. Dependence of transfer coefficients on local stability, J. Fluid Mech., 8 (1960) 529–544.
[10] J. Kondo, O. Kanechika and N. Yasuda, Heat and momentum transfers under strong stability in the atmospheric surface layer, J. Atmos. Sci., 35 (1978) 1012–1021.
[11] G. Schnatz and D. Flothmann, A 'K'-Model and its modification for the dispersion of heavy gases, in: S. Hartwig (Ed.), Heavy Gas and Risk Assessment, Reidel, Dordrecht, 1980, pp. 125–139.
[12] I.E. Idelchik, Handbook of Hydraulic Resistance, 2nd edn., Hemisphere, Washington, DC, p. 170.
[13] D.L. Ermak and M.H. Merry, A methodology for evaluating heavy gas dispersion models, Report UCRL-21025, 1988.